Materials & Design 221 (2022) 110936

Contents lists available at ScienceDirect

Materials & Design

journal homepage: www.elsevier.com/locate/matdes

Residual stress distribution of a locally and inductively quenched and tempered 50CrMo4 steel analysed by synchrotron transmission techniques

V. Jászfi [a,*], P. Prevedel [a], P. Raninger [a], J. Todt [b], D. Mevec [a], Y. Godai [a], E. Maawad [c], R. Ebner [a]

[a] Materials Center Leoben Forschung GmbH, Roseggerstrasse 12, 8700 Leoben, Austria
[b] Chair of Materials Physics of the Montanuniversität Leoben, Jahnstraße 12, 8700 Leoben, Austria
[c] Institute of Materials Physics, Helmholtz-Zentrum Hereon, Max-Planck-Straße 1, 21502 Geesthacht, Germany

HIGHLIGHTS

- Residual stress distribution in locally quenched and tempered 50CrMo4 steel using synchrotron transmission techniques
- Relationship between residual stresses, retained austenite content and hardness for two specific local heat treatment states
- Macrosegregations reduce the magnitude of residual stresses and retained austenite content in the quenched 50CrMo4 steel
- Geometry and quenching rate have a greater influence on the residual stresses than the chemical composition of 50CrMo4 steel

GRAPHICAL ABSTRACT

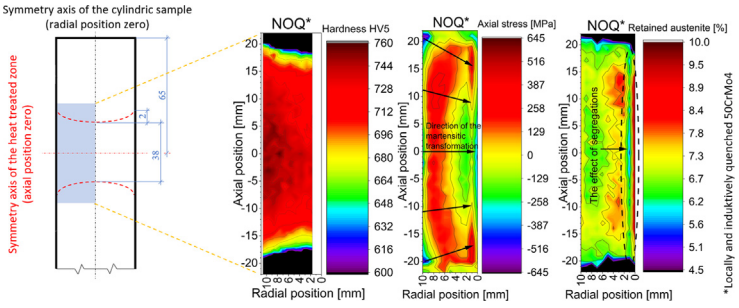

ARTICLE INFO

Article history:
Received 11 April 2022
Revised 29 June 2022
Accepted 8 July 2022
Available online 16 July 2022

Keywords:
Induction heat treatment
Quenching and tempering
50CrMo4
Synchrotron
HE-XRD
Residual stress analysis
Retained austenite
Segregations

ABSTRACT

This work investigates the in-depth residual stress distribution and retained austenite content in plates that were wire eroded from one locally quenched and one locally quenched-tempered 50CrMo4 cylinders by the means of high-energy X-Ray synchrotron transmission techniques. The main challenge was to interpret the results from all diffraction angles to obtain meaningful validation data for future computer simulations of induction hardening and tempering. The results were discussed in relation to hardness distribution. With the help of the applied measurement technique, even the effects of macro-segregation near the longitudinal sample axis can be detected. In inductively heated and quenched cylindrical specimens of 50CrMo4 specimens, macro-segregations near the longitudinal sample axis lead to a reduced retained austenite content, which shifts the axial stresses towards tensile stresses. Comparing the results with those from the literature, it can be seen that variations in the chemical composition of the sample within the specification range of the steel grade have less influence on the residual stress distribution in the induction hardened samples than the sample geometry and/or the quenching rate.

1. Introduction

Induction heat treatment is a field of research that has been studied for a long time and offers wide application possibilities

* Corresponding author.
E-mail address: vince.jaszfi@mcl.at (V. Jászfi).

https://doi.org/10.1016/j.matdes.2022.110936
0264-1275/

due to its short treatment times and high productivity [1]. Surprisingly, it is still not fully understood because of the complex relationships of the steels' microstructure and the electric and electromagnetic properties. These relationships influence the inductive heating of a sample and vice versa. Important material properties (such as hardness, yield strength, toughness) and microstructural features (such as grain size, precipitations, martensite structure) can be specifically influenced by a targeted selection of the inductive heat treatment parameters if the interrelationships for a particular material and its microstructure are fully known. For instance, A. Eggbauer (née Vieweg) studied the effect of different inductive heat treatment parameters in case of a 50CrMo4 steel [2], some relevant results are: Different initial microstructures of 50CrMo4 samples have a notable effect on heating rates and the austenitization process [3]; the different heating rates influence the austenitization and tempering process [4,5] and the cementite/carbide precipitation during tempering [6].

The development of the mechanical properties in 50CrMo4 steel using different induction heat treatment parameters was studied in [7]. There, the authors found that the strength-toughness relationship of a steel can be improved with the right choice of initial microstructure (normalised versus soft annealed) and the appropriate inductive heat treatment parameters (higher tempering heating rates). However, the development and distribution of residual stresses and phase composition for a locally and inductively quenched and quenched-tempered 50CrMo4 was not yet investigated to gain a better understanding of the processes involved. Locally heat treated samples are rarely studied because they involve a complex distribution of microstructure and residual stresses. Both are important parameters in computer simulations of real induction heat treatments to predict the local properties.

There are two main types of strains causing the crystal lattice deformation that leads to residual stresses within a quenched sample: *thermal strains* caused by the different cooling rates experienced by the surface and the interior of the sample and the *transformation strains* due to the volume changes, which occur when austenite transforms into other phases [8]. During heat treatment the strains from inhomogeneous cause stresses, which can locally exceed the elastic limit thus causing plastic deformation. After cooling the remaining elastic stresses and strains trapped within the inhomogeneously plastically deformed material form long-range residual stress fields in the sample or component but also shot-range residual stress fields with crystals.

The development and distribution of these strains and stresses and their origin have been studied in general for a long time [9], although, they seem to be different for each steel composition and heat treatment. J. Todt et al. have analysed the residual stress distribution of a high pressure torsion deformed iron disk by means of High-Energy X-Ray Diffraction (HE-XRD) [10]. They discussed the planar stress gradients measured inside the sample with the present hardness distribution. This HE-XRD analysis method neglects transversal stresses allowing only the analysis of the stresses normal to the beam. Neutron diffraction analysis can determine residual stresses in all three dimensions, as used by Drexler et al. [11], but it only allows an insufficient determination of phase fractions compared to a HE-XRD method. The advantages of using synchrotron techniques are in general the good space- and angle resolution of the diffractions. Additionally, the use of high-energy beams enables the transmission of macro-samples analysing planar in-depth and in-plane microstructure states [12].

The main purpose of this work is to investigate the distribution of the phase fractions of the microstructural elements (e.g. retained austenite) and residual stresses using HE-XRD in transmission mode: a two-dimensional presentation of corresponding results is shown and discussed. This type of analysis for an inductively heated and locally quenched and tempered 50CrMo4 steel is new.

2. Experimental

Two cylindrical (Ø22 × 200 mm) 50CrMo4 steel rods were used in normalised initial state (as received, before heat treatment). The chemical composition of the steel is shown in Table 1. The heat treatment parameters were set considering a previous work [7]. The normalised pearlite-ferrite microstructure of 50CrMo4 is described in detail in [13].

2.1. Performed heat treatments

The time-temperature plot of heat treatment carried out is shown in Fig. 1 (a). The average heating rate (from room temperature to the target temperature of 1050 °C) was chosen to be about 10 K/s. After reaching the Curie temperature, the heating power was increased to keep the heating rate largely constant. The heating frequency was set at 15 kHz for both heat treatments – austenitization and tempering. Quenching was performed using a circumferential water shower unit mounted 50 mm below the inductor with a cooling parameter of $\lambda \approx 0.0341$ (this equals a cooling rate of about 88 K/s) near to the surface. For quenching, the water shower unit was moved to the heat treated region. The temperature inside the rod was measured with type K sheath thermocouples at a distance of 65 mm from the top face of the specimen. The temperature measurement was made both in the centre of the specimen and 2.1 mm below the mantle surface. λ is an industrially commonly used cooling parameter, defined as the cooling time from 800 to 500 °C in seconds divided by hundred. The chosen high cooling rate ensures a definite transformation into a martensitic microstructure. For the additional tempering of the second sample, the heating rate was again chosen to be about 10 K/s and the sample was heated up to 650 °C, followed by cooling in still air. A detailed description of the used induction hardening test rig is given in [7]. The "centre" and "surface" positions indicated in Fig. 1 (a) are the temperatures measured using the previously mentioned type K sheath thermocouples at the centre of the sample and 2.1 mm below the mantle surface, both thermocouples were inserted at a distance of 65 mm from the top face of the sample.

The heating rate and power were determined based on the results from preliminary tests. The specimens were statically heat treated after positioning the centre of the inductor (height 38 mm, inner diameter 36 mm, four windings) at a distance of 65 mm from the top face of the rod, so that the thermocouples were located in the centre of the inductor.

2.2. Preparation of samples for synchrotron measurements in transmission mode

For the investigations, normalised cylindrical 50CrMo4 samples were inductively heat treated. The heat treatment conditions selected were austenitised and quenched (NOQ) on the one hand and austenitised quenched and subsequently tempered (NOQT) conditions on the other. 200 mm long and 3 mm thick plate samples were carefully wire eroded from the centre of the cylindrical samples as illustrated in the sketch in Fig. 1 (b). The final thickness of the samples of 2.5 mm was achieved by fine grinding. Cutting out the flat samples (200 × 22 × 2.5 mm) for the synchrotron investigations from the rods using wire erosion leads to the release of a certain amount of transverse residual stress [10]. This preparation-related change of transversal residual stresses is neglected in this work. However, the original residual stress state

Table 1
The chemical composition of 50CrMo4 steel.

Element	*C*	*Mn*	*Cr*	*Mo*	*Si*	*P*	*S*	*Fe*
50CrMo4 [wt.-%]	*0.49*	*0.71*	*1.05*	*0.18*	*0.27*	*0.016*	*0.01*	*≈97,1*

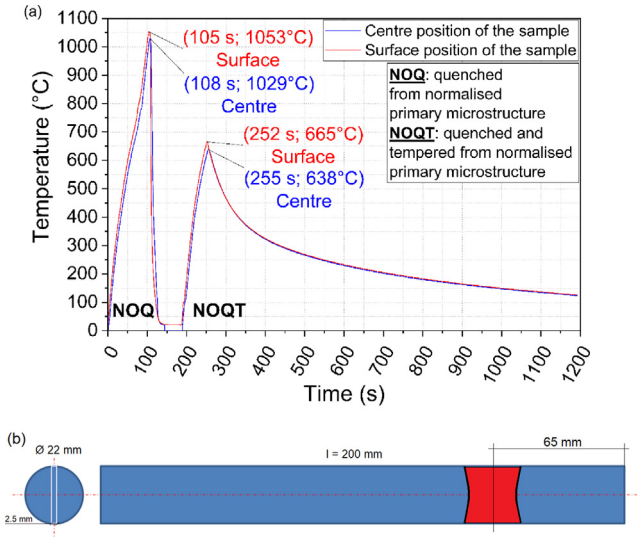

Fig. 1. (a) Time-temperature plot of the local heat treatments performed on the cylindrical 50CrMo4 samples with normalised initial microstructure. Surface = near-surface, 2.1 mm from the surface inside the sample; Centre = temperature in the centre of the sample, 11.0 mm from the surface. NOQ = austenitised and quenched condition (martensitic), NOQT = austenitised and quenched and subsequently tempered condition. (b) Sketch of the sample with the position of the 2.5 mm thick plate eroded from the cylindrical sample (marked with two white lines) and of the heat treated zone (marked in red).

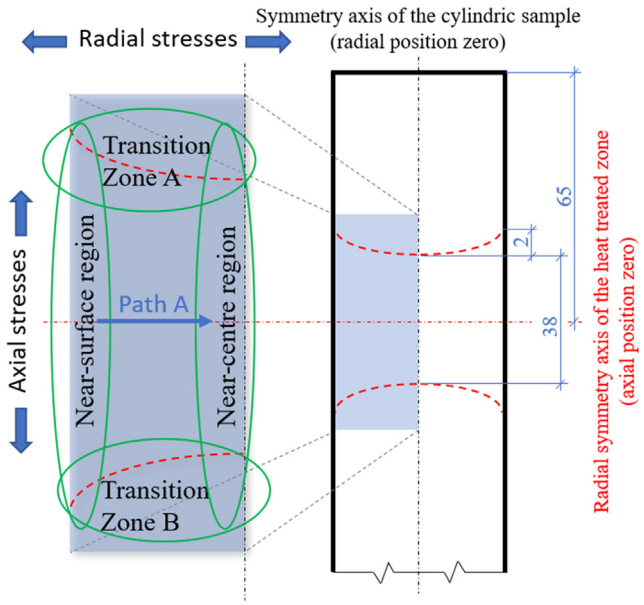

Fig. 2. Schematic representation of the locally heat treated zone (38–42 mm extension in axial direction) of the 2.5 mm thick plate sample with the two symmetry axes and the shaded, light-blue area, where the HE-XRD analyses were performed. This figure is showing a part of Fig. 1 (b) rotated by 90°. The analysed regions and zones are indicated within the analysed area. All subsequent illustrations of the results are positioned symmetrically to both axes of the heat treated zone in radial and axial direction. In addition to the region investigated, the directions of the stresses and the path A are also given, which are of importance in the further course of this work.

in the cylindrical specimen could be approximated by means of finite element method (FEM) simulations.

The shaded light-blue area in Fig. 2 shows the analysed area of the sample around the heat treated zone and a section to highlight details. The austenitised zone extends up to 2 mm beyond the height of the inductor of approx. 38 mm height of the inductor (red dashed lines). Due to the higher heat coupling near the surface and the heat conduction in the sample, the extension of the heat treated zone in axial direction is slightly larger near the edge than in the centre. The heat treated area is separated in distinct zones and regions as also indicated in the Fig. 2. These zones and regions are references for the section "Results and discussion" of this work. All subsequent illustrations of the results show this axially symmetrical half-view of the heat treated zone as illustrated in Fig. 2, and can also generally be considered symmetrical from top to bottom and from left to right.

2.3. Synchrotron measurements in transmission mode

The HE-XRD measurements were performed at the High Energy Materials Science (HEMS) beamline (P07b) at PETRA III [14] using a simple screw clamp sample holder (see Fig. 3). In order to penetrate the 2.5 mm thick samples, high energy X-rays were used with a photon energy of 87.1 keV, corresponding to a wavelength of 0.014235 nm. The beam size was set to 0.1 × 0.1 mm. The resulting transmission diffraction rings were recorded with a Perkin Elmer XRD1621 flat panel 2D detector with an exposure time of 1 s. The detector was placed 1320 mm behind the sample. Conical slits were not used for the experiments, because the analysis of the whole transmission spectrum was required determining also the

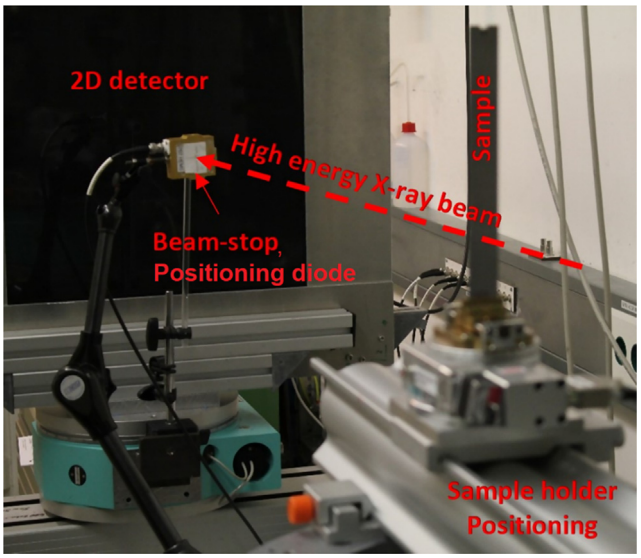

Fig. 3. Measurement setup of the HE-XRD-measurements (Petra III, DESY Hamburg). The beam-stop is behind the positioning diode.

phase fraction of the heat treated area. A pattern of measurements was performed in 1 mm increments, covering half of the symmetric locally heat treated zone. For clearer interpretation, the missing

areas between the measurement points have been interpolated in the representation of the results.

2.4. Other measurements

Vickers HV5 hardness was measured according to EN ISO 6507-1:2006-03 with hardness indentations every 1 × 1 mm in the shaded zone in Fig. 2 using a QNess Q10+ hardness tester. Based on the hardness distribution of inductively austenitised and quenched as well as inductively austenitised and quenched and subsequently tempered 50CrMo4 steel samples, the distribution of residual stresses and retained austenite phase content and their differences in the differently heat treated samples are discussed in more detail. All the analyses were carried out with the same grid arrangement, but the hardness measurements were excluded in a range of 0.5 mm around the longitudinal axis due to the increased segregations there.

Cross-beam scanning electron microscopy device, Zeiss AURIGA® – CrossBeam® workstation and Energy-Dispersive X-ray (EDX) spectroscopy was used with 20 kV acceleration voltage and 10 mm sample distance to prove the existence of the segregations present near the centre of the cylindrical sample.

3. Used evaluation methods

The diffraction data was used for residual stress analysis and determination of retained austenite content. Fig. 4 shows an example of the Debye-Scherrer rings of a single diffraction image and the integrated diffraction pattern of the quenched zone of 50CrMo4. The calculations were performed using the programs Fit2D [15], Matlab [16], Origin [17] and the pyFAI software package [18].

3.1. Residual stress analysis

Residual stresses were evaluated by dividing and integrating Debye-Scherrer rings into 36 azimuthal sections, each 10°wide, subsequently fitting the martensite (ferrite) 110 peak, and finally calculating the elliptical distortion of the ring from the variation of the 2θ position of the peak. This distortion is proportional to the difference between axial and radial stress ($\sigma_{ax} - \sigma_{rad}$) and the method is insensitive to the exact unstrained lattice parameter

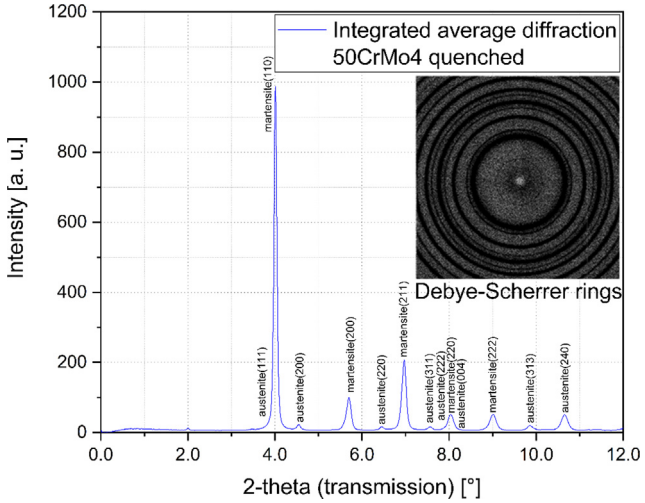

Fig. 4. Example of Debye-Scherrer rings and the integrated intensity pattern (average value over the entire rings) with the indexing of the martensite (ferrite) and austenite peaks of the steel 50CrMo4 in the quenched state (NOQ).

used for evaluation. Assuming that the radial stress is small or negligible, the calculated value approximates the actual axial stress. Therefore, the stress results are referred to as axial stresses in this work. The elastic constant employed for calculation of stress from strain was $\frac{1}{2}S_2^{110,\ martensite} = 5.59 \times 10^{-3}$ GPa^{-1}. For more details please refer to S.C. Bodner et al. [19], where the same approach has been used to determine residual stress maps in similarly sized and microstructurally complex additively manufactured samples.

3.2. Determination of the retained austenite content

To evaluate the austenite phase fraction, selected peaks of ferrite and austenite were fitted using a Pseudo-Voigt function [20]. To minimize the effect of overlapping signals, peaks without adjacent peaks of other phases were chosen. The most probable phases existing in our case are ferrite, austenite and cementite/carbides. For ferrite/bcc (space group: Im-3 m), these were the 200 and 211 peaks, for austenite/fcc (space group: Fm-3 m) the 200 and 220 peaks. The ferrite peak is indicated as martensite in Fig. 4, since the martensite peaks occur at almost the same position as those of the ferritic matrix, despite it being supersaturated with carbon and exhibiting tetragonal distortion. In case of the initial normalized microstructure of 50CrMo4, which is consisting of ferrite and pearlite, the austenite / martensite phase fraction was calculated according to ASTM-E975-13 [21] considering also the estimated 7.5 wt-% cementite phase-content (estimated from the iron-carbon phase diagram assuming all the alloying elements are bound in the cementite of the pearlite).

4. Results and discussion

First, the hardness around the heat treated zone in the inductively austenitised and quenched (hardened only) and in the inductively austenitised and quenched and subsequently tempered condition is discussed. Then the results of the synchrotron analysis, i.e. retained austenite content and residual stresses, are presented and discussed.

4.1. Hardness results

Fig. 5 (a) shows the hardness distribution of the NOQ and NOQT samples using matched scaling. A more detailed view (individual hardness-scaling) of the hardness values of the heat treated region is shown in Fig. 5 (b). The region directly at the centre of the sample was not relevant for the purpose of this work, therefore no results are presented of the area between 0 and 0.5 mm from the centre of the rod.

The shape of the heat treated zone becomes concave towards the centre of the sample (about 2 mm in both directions as also indicated in Fig. 2) indicating a slightly inhomogeneous temperature distribution during austenitization. The accumulation of heat near the surface of the sample is caused by the skin effect. The NOQ sample shows a homogeneous hardness distribution throughout almost the whole hardened volume (Fig. 5 (a)). A slight increase in hardness can be observed towards the surface of the hardened zone, especially in the axial 0-position. The cause is the higher heating intensity and the higher quenching intensity in the surface region, which causes a stable and fine martensite structure with less retained austenite content transforming the austenite in a greater proportion into martensite (as described in [22]). In axial direction, the transition zones from the untreated microstructure to the hardened zone have a width of about 3 mm where the hardness strongly increases from the base level of the original normalised microstructure to the martensite hardness level. The continuously increasing hardness (from about 230 to about 700 HV) in

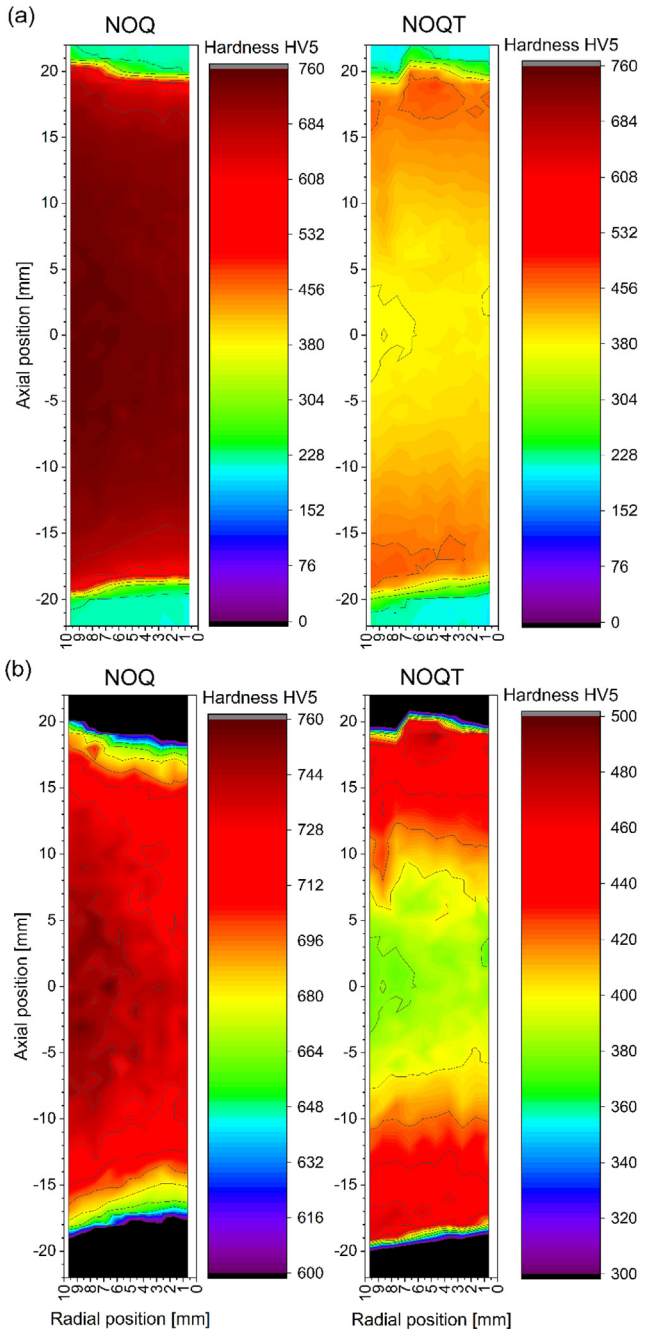

Fig. 5. (a) Hardness mappings (same scaling) of the inductively austenitized and quenched (NOQ) and the inductively austenitised and quenched and subsequently tempered (NOQT) 50CrMo4 steel samples, both were inductively heat treated from normalised initial microstructure, and (b) a finer graded view (different scaling) of the same results.

the transition zones to the heat-treated zone indicates the presence of a mixed microstructure (ferrite, bainite, martensite) in this region. A similar investigation has been conducted by Mevec et al. [23] in the case of an in-depth analysis of an inductive surface hardening process.

In contrast to the NOQT sample, the NOQT sample does not show an increasing hardness towards the surface, but a decreasing hardness in axial direction towards the axial zero position. The kink in the upper transition range that appears in the NOQ sample is probably due to the scattering of the hardness measurements in this transition range. Most noticeable, the NOQT sample is characterised by a zone of lower hardness that increases from the axial zero position towards the untreated regions. Before the hardness drops to the level of the untreated normalised microstructure, there is a thin (ca. 0.5 mm) transition zone of increased hardness (approx. 400–500 HV5 compared to 380 HV5 at the axial zero position), which can be attributed to a reduced tempering temperature, as this is the area where the inductor terminates. This decreasing tempering effect can be observed starting from the axial 5 mm position towards the transition zone. The decreasing tempering temperature with increasing distance from the axial zero position is likely to result in increased dislocation densities, as indicated e.g. in [24].

4.2. Distribution of retained austenite

Depending on the carbon content and the alloying elements of the steel, slow cooling rates during martensite formation can lead to carbon accumulation in the retained austenite, which is thus increasingly stabilised as the cooling rate slows down [25]. It can also be observed in Fig. 6 (a) in the case of the NOQ sample: except in the transition zones, the average retained austenite content is mostly above 6 vol-%. The main alloying elements, Cr and Mo are ferrite stabilisers. Therefore, the retained austenite content is generally expected to be at low levels (under 10 vol-%) in this steel after quenching [8,22].

The more detailed view of the NOQ sample in Fig. 6 (b) shows an increasing retained austenite content towards the centre of the sample in radial direction, which is in line with the previously mentioned fundamentals of the incomplete martensitic transformation. This trend of the increasing retained austenite content is also in line with the trend of the decreasing hardness values of the same sample shown in Fig. 5, especially in the axial zero position from the surface towards the centre of the sample. The only discontinuity in the trend of increasing retained austenite content towards the centre of the sample is a line-shaped zone extending in axial direction of the near-centre region at a distance 1 mm from the centre. Its probable cause of this line-shaped zone is segregation that occurs during the casting of the pre-material.

This segregation affects the martensitic transformation and thus the retained austenite content. Theoretically, an enrichment of the alloying elements Cr and Mn in these segregations would lead to an improved hardenability, which should also increase the hardness in the region. It would explain the decreased retained austenite content (about 3–4 vol-% compared to its neighbouring areas) in this region. The hardness values of this specific region show no measurable hardness increase, therefore, another method, EDX was used to validate the existence of the segregations in this region.

The tempered sample (NOQT) in Fig. 6 (a) shows no significant (detectable) amount of retained austenite except some artefacts caused by the failure of the diffraction peak fitting process of the austenite phase due to insufficient intensity, which are filtered by capping the scale at 2 vol-%.

4.3. The effect of segregations on the retained austenite content

To validate the previously mentioned segregations, present at the 1 mm radial position, EDX measurements were performed. According to [22,24], even a small but significant difference in the chemical composition (particularly the Cr and Fe contents) can prove the existence of segregation in the material. As shown in Fig. 7, the Cr and Fe contents at the radial position of about 1 mm, measured from the longitudinal axis of the sample, differ from those of the adjacent positions. Interestingly, the Cr content is not higher, but lower in this region. However, the difference is very small (about 0.07 wt-%). It disproves the aforementioned pre-

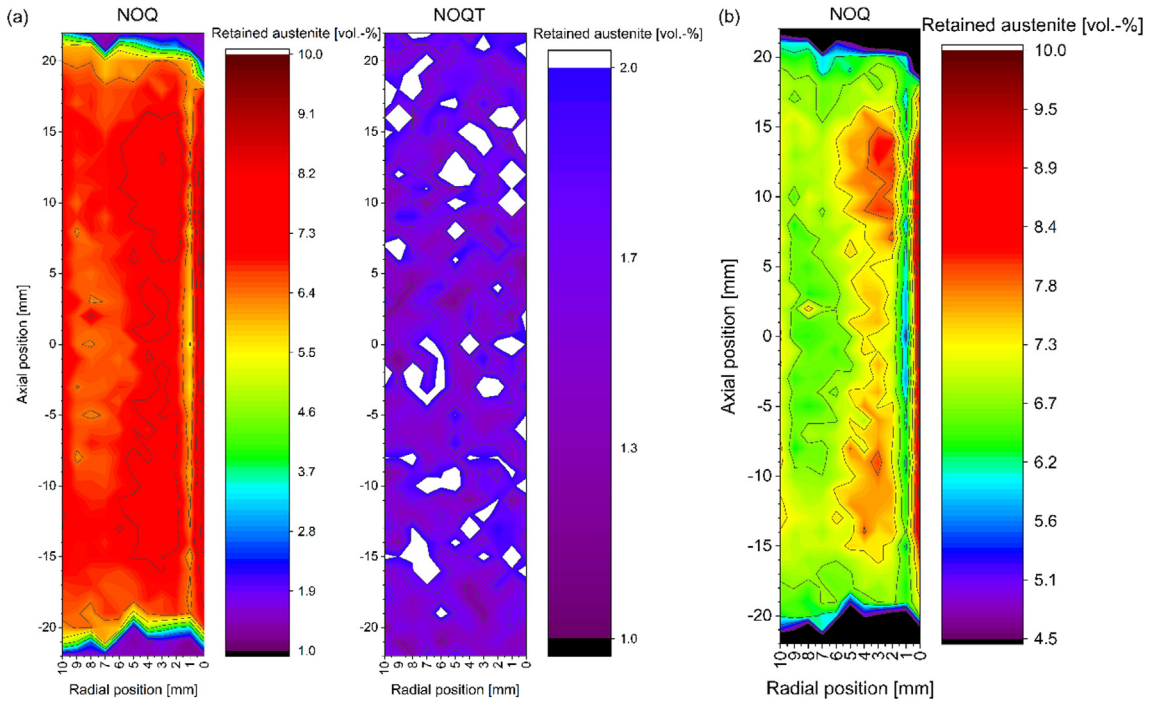

Fig. 6. Comparison of the retained austenite content of (a) the NOQ and NOQT samples (with different scales to filter the errors caused by insufficient intensity of austenite diffraction peak), and (b) a view of the NOQ sample with the scale adjusted to show the variations in retained austenite content within the hardened zone.

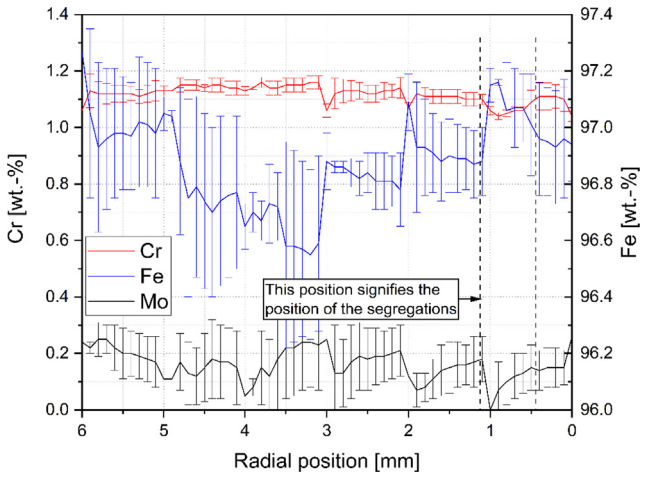

Fig. 7. Check for segregation using an EDX line profile at the axial position zero between the radial positions 0 and 6 mm.

sumptions in the previous section about the enrichment of elements, which assumes a slightly higher hardness in this region. This lower Cr content can be explained due to a higher martensite start and finish temperature, which shifts the retained austenite content in this region to lower levels [26].

4.4. Residual stress distribution

In this section, the results of the NOQ sample are first presented and partly discussed, followed by a comparative discussion of the results of the NOQT sample.

During the quenching process, martensite phase transformation induces compression stresses in the vicinity of austenite crystals and stabilize the retained austenite phase [8]. In a local hardening process, macro-stresses arise in all directions, regardless of the sign of the stresses. Stresses due to temperature gradients can lead to plastification on the one hand and they also influence the transformation strain during phase transformation (TRansformation Induced Plasticity - TRIP) on the other [26].

TRIP is a simplified macroscopic description often used in finite element models addressing two microscopic effects that occur during martensite formation during quenching [27]. The first is the Magee Effect, which describes a martensitic transformation of the austenite grain with a preferred orientation of the martensite variants in the energetically favourable direction. In cases where stresses are present during transformation, the energetically favourable variants are those that lower those stresses. The second is the Greenwood-Johnson Effect, which states that the formation of martensite or other phases causes plastic deformation in the surrounding austenite grains. In the presence of an external load or local stresses the plastic deformation has a preferred orientation. Both effects can lead to a preferred orientation of the strain and cause a macro-elongation of the sample in a preferred direction. Both mechanisms are relevant for the strain history during local quenching but cannot be separated from other relevant strain contributions, unless simulations with special material models are available. In principal, however, the TRIP effect lowers the stresses prevailing at the time of the phase transformation but can contribute to the final residual stresses when the temperature of the component has reached room temperature.

Fig. 8 represents a qualitative depiction of the residual stresses in the NOQ sample. The white regions are all under tensile stresses (hydrostatic) and the black regions are under compressive stresses. During quenching, the narrow near surface region is subjected to continuous water-cooling (quenching) with a cooling rate of ≈ 88 K/s, which forces a rapid martensitic transformation. As shown in Fig. 5 (b), the near-surface region of the heat-treated zone exhibits a slightly higher hardness compared to the core along the radial symmetry axis (path A from Fig. 2). In the case of a perfect through-hardened sample, tensile stresses are expected in the near-surface region [28]. The slightly higher hardness and the somewhat lower residual austenite content in the area near the

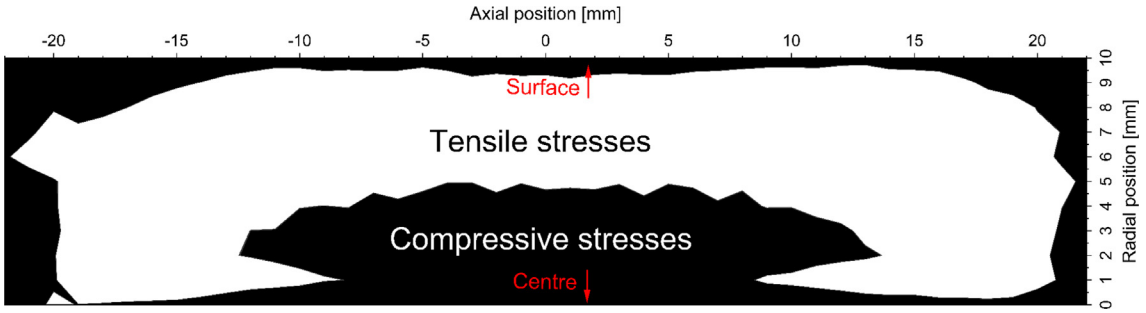

Fig. 8. Black and white representation of the tensile and compressive stress regions in the NOQ sample.

surface indicate that through-hardening did take place but was uneven. The influence of the incompletely transformed initial microstructure (ferrite-pearlite) can be observed in the transition zones where compressive stresses are present indicating the edge of the transformation in the axial direction.

The space between the near-surface region and near-centre region is strongly under tensile stresses up to around 600 MPa that are counterbalancing the compressive stresses caused by the martensitic transformation process along the radial direction towards the centre (the 'C' shape of the tensile stress region in Fig. 8 and Fig. 9). The transformation does not take place instantaneously over the entire cross section, but continuously from the surface towards the centre of the sample. Therefore, when the transformation reaches the near-centre region, the "freshly" transformed martensite there therefore causes tension in the previously transformed region. This region of tensile stresses can build up due to plastic deformation incurred due to uneven plastic deformation caused by the temperature gradients as well as by transformation strain. Towards the centre, a region with compressive stresses occurs again, as the phase transformation comes to a standstill there [9,22,26].

Another representation of the residual stresses is shown in Fig. 9, where the colouring indicates the magnitude of the residual stresses. The arrows indicate the direction in which the martensitic transformation is progressing. The relatively high tensile stresses below the near-surface zone indicate the aforementioned accumulation of stresses in this region.

In the case of the NOQ sample, an interesting region is found at around 1 mm radial position as indicated by the dotted line in Fig. 9, where the tensile stresses appear in the form of a wedge that almost closes the C-shaped region of the tensile stresses. This local axial shift towards tensile stresses can be related to the above-mentioned macrosegregation mentioned caused by casting of the pre-material.

Macrosegregation causes an inhomogeneous distribution of alloying elements, impurities and carbon or a combination of these factors in a sample. A macrosegregation consists of several microsegregations. These microsegregations appear generally at grain boundaries and in the spaces between dendrites upon solidification of the melt as explained in [28]. In segregated regions one or more alloying elements are unevenly distributed. In the present case, the segregated zone has the shape of an almost central line, but this shape depends strongly on the manufacturing process.

In the case of NOQT, the residual stress distribution is rather even. The highest residual stresses remain in the transition regions A and B as indicated in Fig. 2, where the initial microstructure remains partly untransformed. The higher the tempering temperature, the stronger the effects on stress relaxation and reduction of hardness. This is evident from Figs. 5 and 9 where hardness and axial stresses at the axial centre, close to and at path A, are clearly reduced in comparison to the corresponding figures for sample NOQ. Hardness and residual stresses are less affected in the transition zones. The effect of the segregation close to the centre disappears completely in the tempered sample due to stress relief.

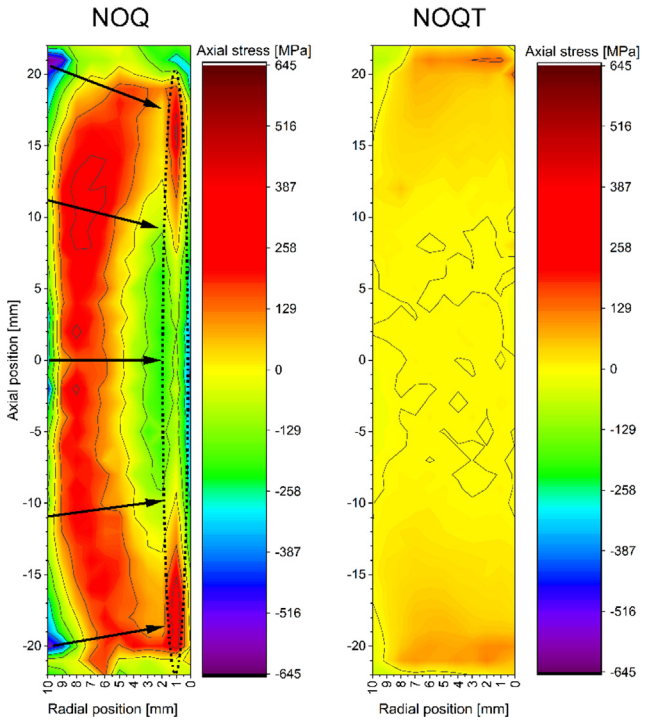

Fig. 9. Comparison of the axial stresses of the samples NOQ and NOQT. The path along which the martensite transformation propagates is marked by arrows in the NOQ sample. The region where segregation occurs is outlined with a dotted line.

4.5. Further discussion of residual stress formation of the NOQ sample

In this section, similar residual stress distributions of previous studies found in the literature will be discussed in relation to our results.

As the review work by Arimoto [9] describes, the development of residual stresses is dependent on the chemical composition of the sample, the shape and diagonal size of the cross-section, the shape of the treated volume/surface and the quenching rate. One of the presented studies in [9] has shown a similar residual stress distribution in the radial direction in the axial zero position for a steel with 8.5% Ni and negligible carbon content. This was a study on the effect of Ni-content on the development of residual stresses in Fe-Ni alloys. This similarity with the results of the present work is interesting because the 50CrMo4 used in present work has no

significant Ni content. The results show that similar residual stress patterns can be achieved for different chemical composition of steels depending on the previously mentioned influencing parameters such as cross-section, shape of the treated volume/surface and quenching rate.

Another review paper by Walton [29] about the distribution of residual stresses of steels explains that compressive stresses are preferred after quenching at the surface, because they provide higher fatigue strength and higher crack resistance of the sample. This is the case for a quenched sample with higher surface hardness (i.e. surface hardening) or thermal treatments such as carburizing and nitriding. Through hardening, in contrast, builds tensile stresses at the surface, but provides a more even hardness distribution in the cross section of the sample. This fact is interesting in our case, because an inductive through-hardening process at low heating rates of 10 K/s shows a not completely homogeneous hardness distributions in radial direction, as shown in Fig. 5(b). This is also supported by the fact that the axial residual stresses near to the surface (shown in Fig. 9) in the quenched state are under compressive stresses, which is common for the surface hardened products as mentioned before. The cause could be the skin effect of the induction heating in this case, which concentrates the heat to the surface region of the sample. The skin depth for induction heating by about 15 kHz for 50CrMo4 is estimated to several μm in the surface region.

Comparable results were also found in a case study [29] of AISI 1045 steel with similar C and Mn contents and a ferritic-perlitic initial microstructure that was quenched from 850 to 20 °C in 11 s under pressurized water. The samples of that cases study had similar geometry to that used in the present work and showed the same residual stress distribution in the radial direction of the symmetry plane. S45C and SAE 1052 steel samples – again with similar C content – investigated in [29] also exhibit this distribution of residual stresses, but with a larger diameter (Ø50, 51 mm) of a cylindrical sample. While these steels all had similar C contents as the one used in this work, their alloying elements differ considerably. This supports the previously stated hypothesis that different chemical compositions (albeit similar C content) of a steel can provide a similar residual stress distribution of a sample by varying the other influencing parameters.

The quenching rate is also an important parameter, which defines the completeness of the martensitic transformation and it can lead to different retained austenite contents of the resulting martensite. This completeness means that the entire austenite phase transforms into martensite, or that part of the austenite phase transforms into bainitic ferrite or ferrite. This can happen, if the cooling rate is not sufficient enough for the martensitic transformation [8,9]. Therefore, the quenching rate is related to the development and distribution of residual stresses, as mentioned previously in this work. A continuous-cooling-transformation (CCT) diagram provides a good basis for the discussion of effect of different quenching rates visualising the phase evolution during the cooling of a specific material and after an austenitizing heat treatment. A reasonably compatible diagram (published in [30]) to the quenching presented in this work has been reused in Fig. 10 with the permission of the authors.

The curves starting from a temperature of about 850 °C at t = 10^{-1} s (T_{start}) in Fig. 10 are the cooling curves with different cooling rates. The hardness achieved in the hardened state is indicated in the circles at the end of these curves. The hardness profile shown in Fig. 5 (a) includes the hardness of the initial structure (about 220 HV), the transition zone and the martensitic hardened zone (about 700 HV). The cooling rate applied in this work was set to about 88 K/s near the surface and 65 K/s near to the centre, which corresponds to an undrawn curve in Fig. 10, which would end at about 10^1 s. This suggests a higher hardness value then

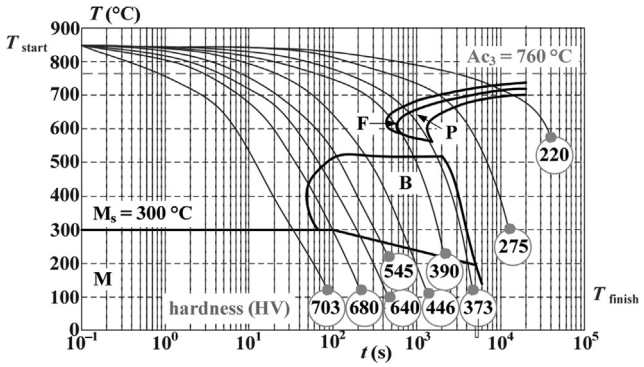

Fig. 10. A CCT diagram of 50CrMo4 (taken from [30]) as a comparison to the presented quenching heat treatment. From the temperature change (dT) over the change of the cooling time (dt), one can calculate the cooling/quenching rate (dT/dt). [30].

the maximum value given in Fig. 10 (max. 703 HV), which is consistent with the results shown in Fig. 5 (max. 760 HV).

The results of these studies from the literature are in line with and supporting/validating the results shown in this work allowing a detailed explanation of the microstructural changes and processes undergoing in 50CrMo4 steel during a local inductive quenching and tempering. These results assist to set an optimal choice of future induction heat treatment parameters for the aforementioned heat treatments and serve as validation data for future computer simulations of similar heat treatments on 50CrMo4 steel.

5. Conclusions

This work presents the results of state-of-the-art analytical methods dealing with the depth distribution of hardness, residual stresses and retained austenite content in an inductively heat treated cylindrical sample of a 50CrMo4 steel. The inductive heat treatment carried out comprises, on the one hand local inductive austenitizing followed by water quenching and, on the other hand inductive austenitizing followed by water quenching and subsequent inductive tempering followed by air cooling.

The following conclusions can be drawn from this work:

- The distribution of residual stresses in axial direction in the cross section of 1) a locally hardened and 2) a locally hardened and tempered steel rod was characterized by specific preparation of plate-like 50CrMo4 samples and HE-XRD using synchrotron radiation in transmission mode. It should be noted that the residual stress state is influenced by the relaxation of the residual stresses in out-of-plane direction, which causes a transverse strain during sample manufacturing. This method was implemented successfully to be able to present the residual stress and retained austenite distribution of the presented heat treatments.
- The local through-hardening causes a complex distribution of a) the hardness, b) the residual stresses and c) the residual austenite phase fractions in the cylindrical samples. The presented heat treatment and characterization results can be used as a complex test case to validate multiphysics simulations of induction heat treatment for general applications of through hardening processes.
- The near-surface region is under strong compression stresses, which are unusual for through-hardening processes. This phenomenon can be caused on the one hand be the skin effect on the other by the volume changes in the centre of the sample at the end of the quenching process forcing the surface towards compression.

- Segregations, stemming from the manufacturing of the material, can be observed in the results of retained austenite content and the residual stresses in axial direction at the inductively austenitized and water quenched heat treated zone. In the segregated areas the retained austenite content is lower and the axial stresses are shifted towards tensile stresses due to their lower Cr and speculated lower C content, causing theoretically the local martensite start and finish temperatures also to higher values.
- Comparing the results with the literature, it can be concluded that the exact chemical composition of the sample has a less significant influence on the residual stress development in the samples than the sample geometry and/or the quenching rate.

Declaration of Competing Interest

The authors declare that they have no known competing financial interests or personal relationships that could have appeared to influence the work reported in this paper.

Acknowledgements

The authors gratefully acknowledge the financial support under the scope of the COMET program within the K2 Center "Integrated Computational Material, Process and Product Engineering (IC-MPPE)" (Project No859480). This program is supported by the Austrian Federal Ministries for Transport, Innovation and Technology (BMVIT) and for Digital and Economic Affairs (BMDW), represented by the Austrian research funding association (FFG), and the federal states of Styria, Upper Austria and Tyrol. Furthermore, the authors would like to thank Mag. Jitka Holcová for processing the synchrotron data.

We acknowledge DESY (Hamburg, Germany), a member of the Helmholtz Association HGF, for the provision of experimental facilities. Parts of this research were carried out at PETRA III and we would like to thank Dr. N. Schell for assistance in using the beamline P07 (The High Energy Materials Beamline), 1st Experimental Hutch (EH1) and its equipment. Beamtime was allocated for proposal H-20010018.

References

[1] V. Rudnev, D. Loveless, R. L. Cook, Handbook of Induction Heating, Second Edition. Boca Raton: CRC Press 772 (2018).
[2] A. Eggbauer, Inductive heat treatment of a 50CrMo4 steel – evolution of microstructure and mechanical properties. Dissertation, Montanuniversität Leoben, Austria, (2018).
[3] V. Jászfi, P. Prevedel, A. Eggbauer, P. Prevedel, D. Mevec, Y. Godai, R. Ebner, Influence of the parameters of induction heat treatment on the mechanical properties of 50CrMo4. HTM – J. Heat Treat. Mater. 74 (2019) 366–379.
[4] A. Eggbauer, M. Lukas, P. Prevedel, M. Panzenbock, G. Ressel, R. Ebner, Effect of the initial microstructure, heating rate and austenitizing temperature on the subsequent formation of martensite and its microstructural features in a QT steel, Steel Res. Int. 90 2 (2019) 1800317, https://doi.org/10.1002/srin.201800317.
[5] A. Eggbauer, M. Lukas, G. Ressel, P. Prevedel, F. Mendez-Martin, J. Keckes, A. Stark, R. Ebner, In-situ analysis of the effect of high heating rates and initial microstructure on the formation and homogeneity of austenite, J. Mater. Sci. 54 (12) (2019) 9197–9212.
[6] A. Vieweg, G. Ressel, P. Raninger, P. Prevedel, S. Marsoner, R. Ebner, Comparing fast inductive tempering and conventional tempering: Effects on the microstructure and mechanical properties. Metall. Res. Technol. 115 No. 407, DOI: 10.1051/metal/2018015 (2018).
[7] A. Vieweg, E. Povoden-Karadeniz, G. Ressel, P. Prevedel, T. Wojcik, F. Martin-Mendez, A. Stark, J. Keckes, E. Kozeschnik, Phase evolution and carbon redistribution during continuous tempering of martensite studied with high-resolution techniques, Mater. Des. 136 (2017) 214–222, https://doi.org/10.1016/j.matdes.2017.09.065.
[8] H.K.D.H. Bhadeshia, R.W.K. Honeycombe, Steels: Microstructure and Properties, Fourth Edition., Elsevier Inc., 2017.
[9] K. Arimoto, in: Encyclopedia of Iron, Steel, and Their Alloys, CRC Press, 2016, pp. 3605–3633.
[10] J. Todt, J. Keckes, G. Winter, P. Staron, A. Hohenwarter, Gradient residual strain and stress distributions in a high pressure torsion deformed iron disk revealed by high energy X-ray diffraction, Scripta Materialia. 146 (2018) 178–181.
[11] A. Drexler, W. Ecker, R. Hessert, B. Oberwinkler, H. Gänser, J. Keckes, M. Hofmann, A. Fischersworring-Bunk, Finite element modeling of the residual stress evolution in forged and direct-aged alloy 718 turbine disks during manufacturing and its experimental validation, AIP Conf. Proc. 1896 (2017) 070001, https://doi.org/10.1063/1.5008076.
[12] P.J. Withers, M. Turski, L. Edwards, P.J. Bouchard, D.J. Buttle, Recent advances in residual stress measurement, Int. J. Press. Vess. Pip. 85 (3) (2008) 118–127.
[13] J. Orlich, A. Rose, P. Wiest, Atlas zur Wärmebehandlung der Stähle. Bd. 3, Verl. Stahleisen, Düsseldorf, ISBN-13: 978-3514001336 (1973).
[14] N. Schell et al, The high energy materials science beamline (HEMS) at PETRA III. In Materials Science Forum 772, 57–61 (Trans Tech Publications Ltd, 2014).
[15] Website, https://www.esrf.eu/computing/scientific/FIT2D/, taken on 31.07.2020.
[16] Website, https://de.mathworks.com/products/matlab.html, taken on 31.07.2020.
[17] Website, https://www.originlab.com/, taken on 31.07.2020.
[18] G. Ashiotis, A. Deschildre, Z. Nawaz, J.P. Wright, D. Karkoulis, F.E. Picca, J. Kieffer, The fast azimuthal integration Python library: pyFAI, J. Appl. Cryst. 48 (2) (2015) 510–519.
[19] S.C. Bodner, L.T.G. van de Vorst, J. Zalesak, J. Todt, J.F. Keckes, V. Maier-Kiener, B. Sartory, N. Schell, J.W. Hooijmans, J.J. Saurwalt, J. Keckes, Inconel-steel multilayers by liquid dispersed metal powder bed fusion: Microstructure, residual stress and property gradients, Add. Manuf. 32 (2020) 101027.
[20] W.I.F. David, Powder diffraction peak shapes. Parameterization of the pseudo-Voigt as a Voigt function, J. Appl. Crystall. 19 (1) (1986) 63–64.
[21] ASTM-E975-13, Standard Practice for X-Ray Determination of Retained Austenite in Steel with Near Random Crystallographic Orientation, ASTM International, West Conshohocken, PA, www.astm.org (2013).
[22] T. Cain, Hardening, Tempering and heat treatment. Argus Books ISBN-13 : 978-0852428375 (1984).
[23] D.G. Mevec, P. Raninger, P. Prevedel, V. Jászfi, A Posteriori Reconstruction of the Temperature Distribution in Surface Hardened Tempering Steel, Sci. Rep. 10 (2020) 7481, https://doi.org/10.1038/s41598-020-63328-6.
[24] H. Zhou, Q. Zhang, B. Yi, J. Wang, Hardness prediction based on microstructure evolution and residual stress evaluation during high tensile thick plate butt welding, Int. J. Naval Archit. Ocean Eng. 12 (2020) 146–156.
[25] G. Kraus, Steels Processing, Structure, and Performance, Second Edition, ASM International, ISBN-13: 978-1-62708-083-5 (2015).
[26] D. E. Laughlin, & K. Hono, Physical Metallurgy: Volume 3. ELSEVIER 2899, ISBN: 978-0-444-89875-3 (2014).
[27] J.B. Leblond, G. Mottet, J.C. Devaux, A theoretical and numerical approach to the plastic behaviour of steels during phase transformations—I. Derivation of general relations, J. Mech. Phys. Solids 34 (4) (1986) 395–409.
[28] E.J. Pickering, Macrosegregation in steel ingots: the applicability of modelling and characterisation techniques, ISIJ Int. 53 (6) (2013) 935–949.
[29] H.W. Walton, Deflection Methods to Estimate Residual Stress. Handbook of Residual Stress and Deformation of Steel G. Totten, M. Howes, T. Inoue, editors, p89-98 DOI: 10.1361/hrsd2002p089 (2002).
[30] V. Kotlan, D. Pánek, R. Hamar, Modelling of laser heating with induction pre-heating and post-heating and its experimental verification, in: IECON 2014–40th Annual Conference of the IEEE Industrial Electronics Society, 2014, pp. 3246–3251, https://doi.org/10.1109/IECON.2014.7048976.